PHYSICAL REVIEW B VOLUME 36, NUMBER 14 15 NOVEMBER 1987-I

Primary-energy dependence of the momentum transfer in reflection inner-shell-electron energy-loss spectra of layered transition-metal dichalcogenides

Youichi Ohno
Department of Physics, Faculty of General Education, Utsunomiya University, 350 Mine-machi, Utsunomiya 321, Japan
(Received 19 January 1987)

Sulfur $L_{2,3}$ and titanium $L_{2,3}$ and $M_{2,3}$ inner-shell-electron energy-loss spectra in $1T$-TiS_2, $1T$-$TiSe_2$, $2H$-TaS_2, and $2H$-MoS_2 have been measured at various primary energies in the reflection mode. A remarkable primary-energy dependence is found. As the primary energy decreases, the first peak that is assigned to the unoccupied t_{2g} band for the $1T$ compounds and to the unoccupied d_{z^2} band for $2H$-TaS_2 increases in intensity relative to the second peak. The peak positions are almost unchanged. They are in agreement with those of band-structure calculations and x-ray absorption spectra. The primary-energy dependence has been discussed mainly in terms of the breakdown of dipole selection rules due to momentum transfer involved in the inelastic scattering process and anisotropy in electronic structures.

I. INTRODUCTION

Inner-shell-electron energy-loss spectroscopy (ISEELS) or core-level-electron energy-loss spectroscopy (CEELS) becomes more and more important and many workers investigate the near-edge structures and the extended fine structures because it gives information about chemical composition, electronic structure, and atomic arrangement in the bulk and at the surface.[1] Recently interesting behavior has been found in reflection ISEELS spectra, that is, shape variation, energy shift, and appearance of new structures.

Powell and Erickson[2] measured the $M_{2,3}$ ISEELS spectra of vanadium at various primary energies and found that the near-edge structures varied and the threshold shifted with primary energy. The similar variation and energy shift were observed by Sakisaka *et al.*[3] for the $M_{2,3}$ ISEELS spectra of Cr and Fe. The former attempted to interpret the variation and the energy shift in terms of the transition from sudden to adiabatic excitation of inner-shell electrons and exchange interaction between incident and target electrons. The latter explained the similar phenomena in terms of recombination and postcollisional interaction.

Kanski and co-workers[4] and Strasser and co-workers[5] measured the $M_{4,5}$ ISEELS spectra of rare-earth metals as a function of primary energy and found systematic variations in intensities of the two peaks observed in each spin-orbit component. The former proposed a dynamic screening mechanism involving an intermediate, screened, quasilocalized state to interpret the variations. The latter, however, showed that they were explained in terms of the multiplet structure and the breakdown of dipole selection rules by referring to the theoretical calculation of Esteva and Karnatak.[6] Recently, Netzer and Karnatak[7] showed that the latter explanation was reasonable for the interpretation of new peaks appeared in the $N_{4,5}$ ISEELS spectra of rare-earth metals measured at low primary energies.

Leapman and co-workers[8] and Saito *et al.*,[9] investigated the angular dependence of the transmission ISEELS spectra of anisotropic materials such as graphite and boron nitride. They found that the peak intensities of the near-edge structures varied, depending on the parallel and perpendicular components of momentum transfer to the c axis and reflecting anisotropy in electronic band structures. Recently Papagno and co-workers[10] suggested that a similar result could be obtained from the primary-energy dependence of the reflection ISEELS spectra.

This paper presents the sulfur $L_{2,3}$ and the titanium $M_{2,3}$ and $L_{2,3}$ ISEELS spectra in $1T$-TiS_2, $1T$-$TiSe_2$, $2H$-TaS_2, and $2H$-MoS_2 as a function of primary energy. The notations $1T$ and $2H$ are used to distinguish different polymorphs and polytypes. In a $1T$ structure each transition metal is octahedrally coordinated to six sulfur atoms while in a $2H$ structure it is trigonal-prismatically coordinated. The difference in coordination leads to different ligand-field splitting of metal d levels. In a $1T$ structure they are split into two parts, i.e., t_{2g} ($d_{z^2}, d_{x^2-y^2}, d_{xy}$) and e_g (d_{xz}, d_{yz}). In a $2H$ structure they are split into three different energy parts, i.e., d^{z^2}, $d_{x^2-y^2}$ and d_{xy}, and d_{xz} and d_{yz}. Here the z orientation coincides with the c axis. Since the compounds crystallize in layer-type structures with fairly strong intralayer covalent bonding and weak interlayer van der Waals bonding, they exhibit anisotropic electrical and optical properties, having quasi-two-dimensional energy band structures.[11] Because many band calculations and optical experiments have been done for the compounds, they are appropriate not only to investigate information obtained from reflection ISEELS spectra but also to confirm the suggestion of Papagno and co-workers.

The near-edge structures will be discussed, compared with band calculations and other optical spectra obtained by means of x-ray-absorption spectroscopy (XAS), appearance-potential spectroscopy (APS), and inverse-photoemission spectroscopy (IPS). The primary-energy

dependence will be discussed mainly in terms of momentum transfer, its parallel and perpendicular components to the surface, and anisotropy in electronic band structures.

II. EXPERIMENTS

Figure 1 shows the schematic diagram of our apparatus used here. A double-pass cylindrical mirror analyzer (PHI Model No. 15-255G) equipped with a coaxial normal incidence electron gun was employed to measure the reflection ISEELS spectra as well as the electron spectroscopy for chemical analysis (ESCA) spectra and the Auger-electron-spectroscopy (AES) spectra. The measurements were performed in the second-derivative mode at modulation voltage of 1 V peak to peak. The single crystals of TiS_2, $TiSe_2$, TaS_2, and MoS_2 were prepared by high-temperature reaction from elements in stoichiometric amounts in an evacuated and then closed silica ampoule. The perfect and clean surfaces were prepared by cleavage in the atmosphere just before the measurements. Since the compounds are made up of the regular stacking of covalently bonded chalcogen-metal–chalcogen sandwich layers and weakly-bonded van der Waals gaps, then the cleavage occurs at van der Waals gaps perpendicular to the c axis. Sample exchange was made for a short time without disturbing the vacuum level in the main chamber, using a specimen introduction system. The argon-ion sputtering and subsequent annealing technique for surface cleaning was not used because of surface disturbance and departure of a chemical composition from a stoichiometry. AES measurements were carried out in UHV of the order of 10^{-8} Pa just before the ISEELS measurements. The spectra displayed a small carbon peak (about a few percent of a substrate signal), but the other contaminations were not detected.

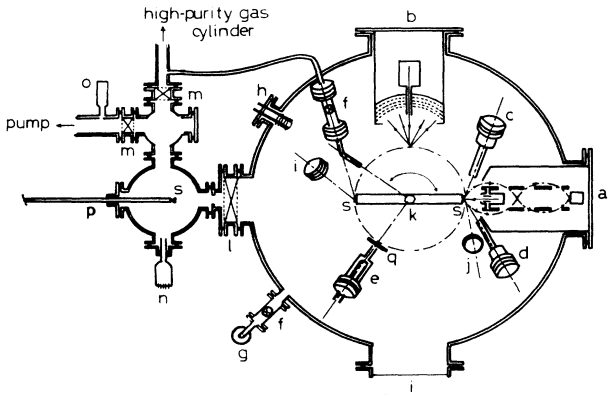

FIG. 1. Schematic diagram of our UHV system; (a) double-pass CMA, (b) low-energy electron diffraction (LEED) plus AES optics, (c) grazing-incidence electron gun, (d) argon-ion gun, (e) evaporator, (f) leak valve, (g) high-purity argon gas, (i) window, (j) spare port for an x-ray tube, (k) manipulator, (l) gate value, (m) butterfly valve, (n) ionization gauge, (o) Pirani gauge, (p) specimen introduction system, (q) shutter, (s) sample position.

Figure 2 shows the schematic diagram of our data acquisition and processing system used in both ISEELS and AES measurements. The upper lines show the system employed in the modulation voltage mode. This mode is useful not only for a rapid analysis of a chemical composition with large-beam current but also for obtaining directly the first- and the second-derivative spectra. The middle line shows the system employed in the pulse-counting mode. This mode is useful for the measurements of $N(E)$ spectra with small-beam current as low as 0.01 μA or less. In both cases the data obtained by repeated measurements were processed with a personal computer (Nippon Electric Corporation 9801F3) via an analog-digital (AD) converter and the final data were output on both a printer and an X-Y plotter as averaged and normalized intensity versus energy. The details of our apparatus and our data acquisition and processing system have been described in a previous paper.[12]

III. RESULTS

Figure 3 shows the sulfur $L_{2,3}$ and the titanium $M_{2,3}$ and $L_{2,3}$ ISEELS spectra in TiS_2. For a comparison the sulfur K XAS spectrum is also shown. The spectra are drawn by aligning the excitation thresholds which correspond to the first minimum for the second-derivative ISEELS spectra and to the inflection point of the initial rise of absorption for the XAS spectrum. The origin of the horizontal axis is the excitation threshold of each spectrum. The fine structures observed around 30 eV in the Ti $M_{2,3}$ spectrum arises from excitation of titanium M_1 electrons. The Ti $L_{2,3}$ spectrum, on the other hand, exhibits a doublet structure arising from core-level splitting due to spin-orbit interaction, the energy separation being 6.3 eV, somewhat larger than those of Bearden and Burr[13] (6.0±0.8 eV), Cardona and Ley[14] (6.1 eV), and Leapman *et al.*[15] (5.5 eV). This relatively small splitting may result in the overlap between the near-edge structures of their components. The S $L_{2,3}$ ISEELS spectrum is quite similar to the S K XAS spectrum in

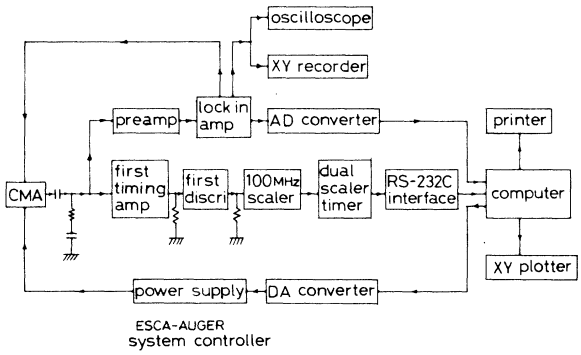

FIG. 2. Schematic diagram of our data acquisition and processing system. The system in the upper lines is employed in the modulation voltage mode, while the system in the middle line is employed in the pulse-counting mode. The scanning voltage applied to the CMA is controlled by a personal computer (in the bottom line).

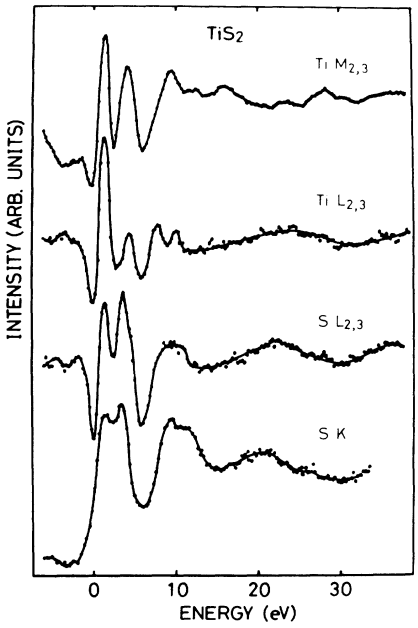

FIG. 3. Titanium $M_{2,3}$ and $L_{2,3}$ and sulfur $L_{2,3}$ ISEELS spectra in TiS_2. They were measured in the second-derivative mode. For a comparison, the sulfur K XAS spectrum is also shown (bottom spectrum). The origin of the horizontal axis is the excitation threshold of each spectrum.

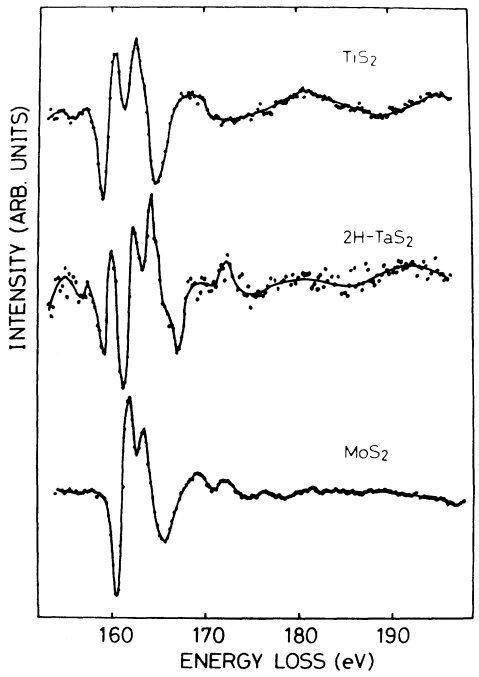

FIG. 4. Comparison among the sulfur $L_{2,3}$ ISEELS spectra in $1T$-TiS_2, $2H$-TaS_2, and $2H$-MoS_2. They were measured in the second-derivative mode. The energy of the incident electrons was 260 eV.

which the near-edge structures consist of two peaks near the threshold and a broad peak at higher energy. These features can be explained qualitatively in terms of the energy band structures. The assignments have been carried out in a previous paper.[16] According to the results, the two peaks near the threshold arise from the transitions of inner-shell electrons to unoccupied Ti $3d$ t_{2g}, and e_g bands which are admixed with sulfur $3p$ orbitals, while the broad peak arises from the transitions to unoccupied Ti $4s4p$ bands. The t_{2g}-e_g separation evaluated from the S $L_{2,3}$ ISEELS spectrum is 2.3 eV, in good agreement with the theoretical values of Zunger and Freeman[17] and Benesh *et al.*[18] and with the experimental values obtained from XAS (Refs. 16 and 19) and APS (Ref. 20) spectra, but those from the Ti $L_{2,3}$ and the Ti $M_{2,3}$ ISEELS spectra are slightly larger. A good agreement is found in energy positions of the first peak and second and third minima, suggesting that these spectra reflect the same energy band structures of TiS_2.

Figure 4 shows the comparison among the S $L_{2,3}$ ISEELS spectra in $1T$-TiS_2, $2H$-TaS_2, and $2H$-MoS_2. In the $2H$ compounds metal d levels are split into three levels by ligand field as described above and Mattheiss[21] has indicated the importance of interband hybridization of d_{z^2}, $d_{x^2-y^2}$, and d_{xy} bands. This hybridization results in a narrow d sub-band as it is called a "d_{z^2}" band. This band is the lowest energy band among the d subbands and has two electrons occupancy per chemical formula, so that it is half-filled for TaS_2, the group-V compound and completely filled for MoS_2, the group-VI compound. If the first peak for TaS_2 is assigned to the unoccupied "d_{z^2}" band and the next two peaks to the remaining d subbands, we can easily understand the disappearance of the first peak in the MoS_2 spectrum.

In the above discussion we neglected the influence of core-level splitting on the S $L_{2,3}$ and the Ti $M_{2,3}$ spectra. The splitting of the S $L_{2,3}$ levels has been determined from an XAS study[22] to be 1.2 eV. Nevertheless the near-edge structures are well correlated with the band-structure calculations and the sulfur K XAS spectrum.

To investigate the primary-energy dependence of the near-edge structures, the S $L_{2,3}$ and the Ti $M_{2,3}$ and $L_{2,3}$ ISEELS spectra in TiS_2, TaS_2, and MoS_2 are shown as a function of primary energy in Figs. 5–9. All the spectra were measured in reflection geometry at normal incidence. Here attention must be paid that the spectral resolution is reduced with increasing the primary energy owing to the inherent nature of the analyzer, although the measurements have been carried out at the same modulation voltage of 1 V (peak to peak). We find that the first peak of the S $L_{2,3}$ and the Ti $M_{2,3}$ and $L_{2,3}$ spectra in TiS_2 decreases in intensity with increasing the primary energy. Especially for the S $L_{2,3}$ and Ti $M_{2,3}$ spectra the intensity ratio of the first peak to the second peak becomes inverse. Similar behavior is observed for the first peak of the S $L_{2,3}$ ISEELS spectrum in TaS_2 (see Fig. 8). The peak which has been assigned to the "d_{z^2}" band decreases in intensity with primary energy and almost disappears at $E_p = 600$ eV. On the other hand, the near-edge structures of MoS_2 are not so greatly changed (see Fig. 9). The features of the S $L_{2,3}$ and Ti

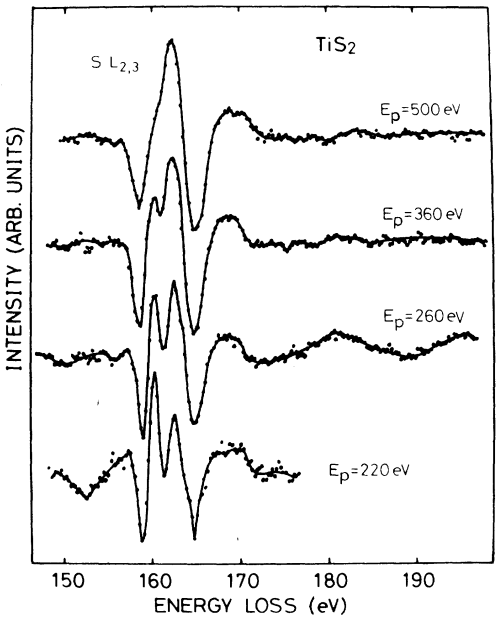

FIG. 5. Sulfur $L_{2,3}$ ISEELS spectra in TiS_2 at various primary energies. They were measured in the second-derivative mode in reflection geometry at normal incidence.

energies are similar to those of the corresponding XAS (Ref. 19) and APS (Ref. 20) spectra (no comparison is made for the Ti $M_{2,3}$ spectrum because up to date no Ti $M_{2,3}$ XAS and APS spectra have been obtained), while

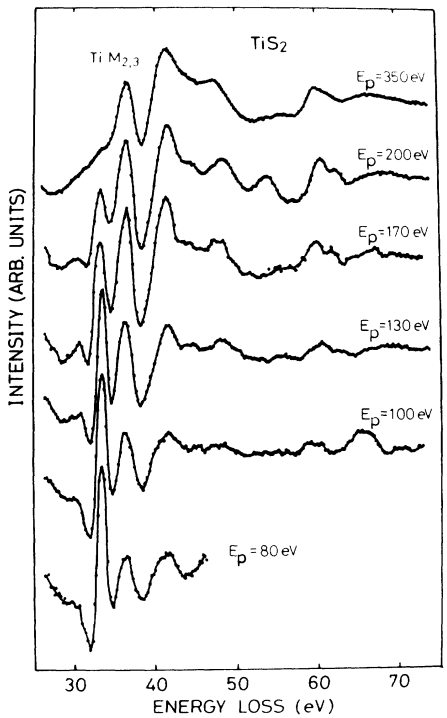

FIG. 6. Titanium $M_{2,3}$ ISEELS spectra in TiS_2 at various primary energies. They were measured in the second-derivative mode in reflection geometry at normal incidence.

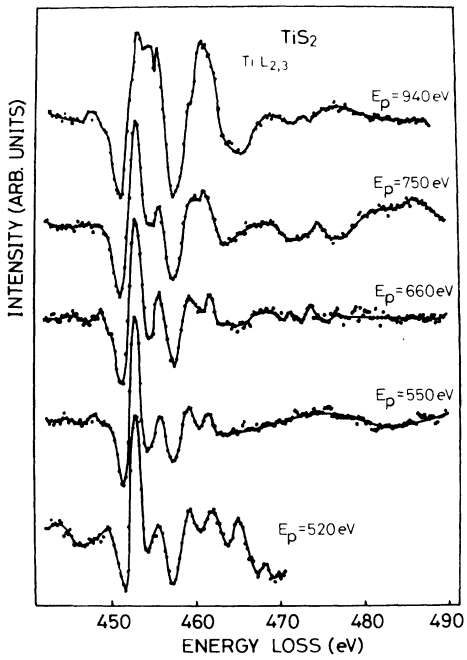

FIG. 7. Titanium $L_{2,3}$ ISEELS spectra in TiS_2 at various primary energies. They were measured in the second-derivative mode in reflection geometry at normal incidence.

the features at lower primary energies resemble those of the IPS spectrum at normal incidence. In Fig. 10 the Ti $L_{2,3}$ ISEELS spectra in TiS_2 and $TiSe_2$ measured at $E_p = 530$ eV are compared with the IPS spectrum[23] of $TiSe_2$.

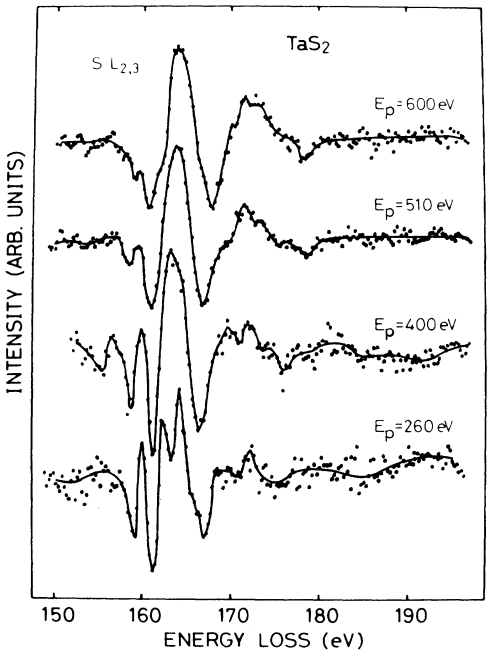

FIG. 8. Sulfur $L_{2,3}$ ISEELS spectra in TaS_2 at various primary energies. They were measured in the second-derivative mode in reflection geometry at normal incidence.

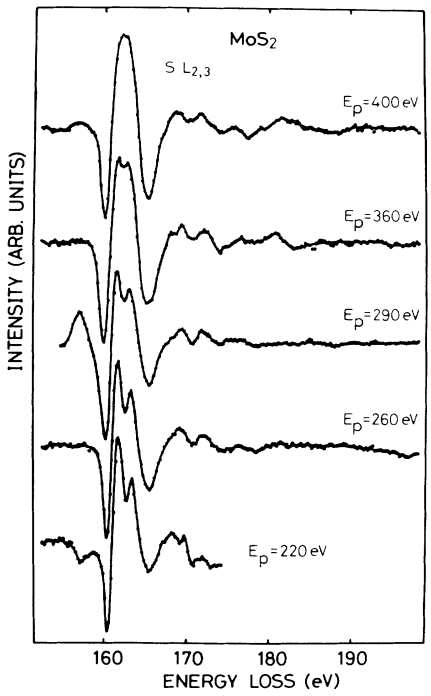

FIG. 9. Sulfur $L_{2,3}$ ISEELS spectra in MoS_2 at various primary energies. They were measured in the second-derivative mode in reflection geometry at normal incidence.

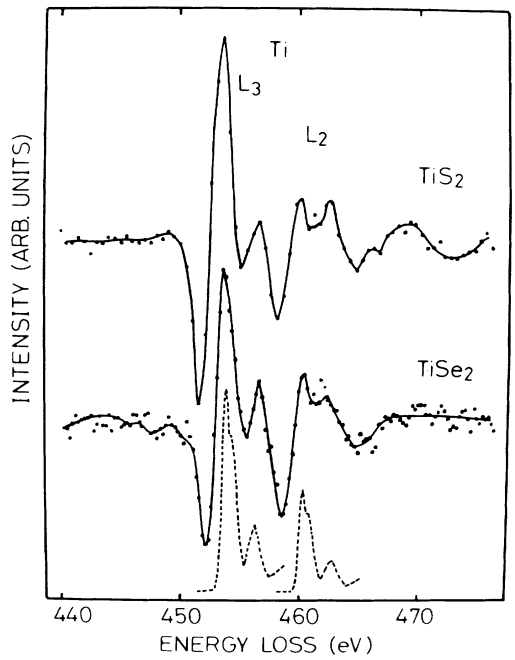

FIG. 10. Comparison among the titanium $L_{2,3}$ ISEELS spectra in TiS_2 and $TiSe_2$ and the IPS spectrum of $TiSe_2$. The ISEELS spectra were measured at $E_p = 530$ eV in the second-derivative mode at normal incidence. The IPS spectrum was measured at $E_p = 13.25$ eV at normal incidence (Ref. 23). This spectrum was drawn repeatedly at the distance of $L_{2,3}$ core-level splitting of 6.5 eV and the intensity ratio was 2 as expected from the electron populations (broken line).

IV. DISCUSSION

The following factors should be considered in discussing the primary energy dependence observed in reflection ISEELS spectra measured by slow incident electrons; (1) surface effects, (2) exchange interaction, (3) postcollisional interaction, (4) dynamic screening, and (5) momentum transfer.

(1) Surface effects. Since the mean free path of incident electrons is reduced with decreasing the primary energy in our energy region, surface effects become more important for the spectra at lower primary energies. However, the cleavage surfaces used here are perfect and quite inactive as described in Sec. II. Then we may neglect the effects.

(2) Exchange interaction. In threshold excitation of inner-shell electrons by slow-incident electrons, exchange interaction occurs between an inner-shell hole and a localized valence electron and between an incident electron and a localized target electron. Even if the former exchange interaction exists and causes the multiplet structures as observed in XAS and XPS spectra of ionic transition-metal and rare-earth compounds,[24,25] it does not depend on primary energy. On the other hand, the latter exchange interaction depends on primary energy and affects the transitions involving a change in the spin multiplicity. Hence the interaction results in the shape variations, allowing optically-forbidden transitions such as $1^1S \rightarrow 2^3S$ and $1^1S \rightarrow 2^3P$ transitions.[26] Since the transition probabilities depend on the overlap between the initial- and the final-state wave functions, the interaction may be significant for a slow-incident electron and a strongly localized target electron. In the case of $1^1S \rightarrow 2^3S$ excitation in a helium atom by 225 eV electron impact, for example, the peak intensity is about three orders of magnitude less than that for the optically-allowed $1^1S \rightarrow 2^1P$ transitions.[26] Taking delocalization of d electrons in layered transition-metal dichalcogenides into account, we may conclude that the above drastic change in our spectra cannot be explained by only the interaction.

(3) Post-collisional interaction. This interaction is a kind of dynamic screening. In threshold excitation of an inner-shell electron by a slow-incident electron, two slow electrons are produced, leaving a core hole, i.e., an inelastically-scattered electron and an excited electron. The latter electron with small kinetic energy partially screens the core hole. Then the scattered electron feels a smaller attractive potential. As a result, the excitation threshold shifts to lower energy. In our spectra, however, such a shift cannot be found. Therefore we may neglect the interaction.

(4) Dynamic screening. The dynamic screening mechanism involving the creation of a screened intermediate state has been proposed by Kanski and Wendin[4] to interpret the intensity variations of the doublet structure observed in each spin-orbit component of the $M_{4,5}$ ISEELS spectra of Ba, La, and Ce. Following their interpreta-

tion, the variations for La, for example, are caused by the transition from the $3d \rightarrow 4f$ excitation process involving a decay of a screened, intermediate $3d^9 4f^2$ state to the direct $3d \rightarrow 4f$ excitation process. Kanski and Wendin have considered that the former is dominant for slow-incident electrons while the latter is dominant for fast-incident electrons. At present it cannot be found if such an effect has influence on our spectra or not. However, it is worth noting that the peak positions of the near-edge structures are consistent with those of the band calculations and the XAS spectra unlike the case of Kanski and Wendin. Recently, Esteva and Karnatak[6] and Matthew *et al.*[5] showed that the intensity variation of the La $M_{4,5}$ ISEELS spectrum can be successfully explained in terms of the multiplet structures and the breakdown of dipole selection rules due to momentum transfer which is involved in inelastic scattering.

(5) Momentum transfer. If surface effects, exchange interaction, post-collisional interaction, and dynamical screening are negligibly small, the differential cross section for excitation of an inner-shell electron from an initial state $|i\rangle$ to a final state $|f\rangle$ is written within the single-electron model and the first Born approximation and correlated to the generalized oscillator strength (GOS) defined by[27]

$$f_{if}(\Delta E,q)=\frac{2m\,\Delta E}{\hbar^2 q^2}\sum_f \left|\left\langle f\left|\sum_j e^{i\mathbf{q}\cdot\mathbf{r}_j}\right|i\right\rangle\right|^2 \times\delta(E_f-E_i-\Delta E)\ , \tag{1}$$

where q is the momentum transfer, ΔE the energy loss, m the free electron mass, $\hbar$ the Planck constant divided by 2π, and $\mathbf{r}_j$ the position vector of the electron participating in the transitions. If inelastic scattering occurs with small-momentum transfer, the operator $e^{i\mathbf{q}\cdot\mathbf{r}_j}$ may be expanded as follows:

$$e^{i\mathbf{q}\cdot\mathbf{r}_j}=1+i\mathbf{q}\cdot\mathbf{r}_j-(\mathbf{q}\cdot\mathbf{r}_j)^2+\cdots\ . \tag{2}$$

The first term on the right side does not contribute to the GOS, the second term causes the dipole transitions identical to the optical transitions by polarized light, and the third term causes the quadrupole transitions which are optically forbidden. Thus polarization selection rules still hold with respect to the direction of momentum transfer, but dipole selection rules are relaxed.

If forward inelastic scattering makes a dominant contribution to the reflection energy-loss spectra as shown in the Appendix, we may consider that most of the inelastic events occur at small scattering angles and the energy losses observed during reflection from a surface are accompanied by large elastic collision. This model has already been proposed by Nassiopolous and Cazaux.[28] The outline is illustrated schematically in Fig. 11. The notations O and O' represent the points at which the inelastic event occurs before and after elastic collision. The notation P represents the elastic event. For simplicity we may treat the energy loss process which involves the inelastic event with a small scattering angle $\Delta\theta$ and the elastic event with a large scattering angle θ, the total scattering angle being 137.7, which is determined from the angular aperture of the CMA. The incident electron undergoes energy and momentum transfer in such a way that the conservation rules are fulfilled. For a simple calculation, the momentum transfer is then given by

$$q=\frac{\sqrt{2m}}{\hbar}[2E_p-\Delta E-2E_p^{1/2}(E_p-\Delta E)^{1/2}\cos\Delta\theta]^{1/2}\ , \tag{3}$$

where E_p is the primary energy. For the inelastic event before elastic collision its parallel and perpendicular components to the surface are, respectively, given by

$$k''_{\text{pre}\parallel}=q\sin\alpha=\frac{\sqrt{2mE_p}}{\hbar}\left[1-\frac{\Delta E}{E_p}\right]^{1/2}\sin(\Delta\theta) \tag{4}$$

and

$$k''_{\text{pre}\perp}=q\cos\alpha=\frac{\sqrt{2mE_p}}{\hbar}\left[1-\left[1-\frac{\Delta E}{E_p}\right]^{1/2}\cos(\Delta\theta)\right]\ , \tag{5}$$

where α is the angle between the wave vector of the incident electron $\mathbf{k}_{p\cdot\text{pre}}$ and the momentum transfer vector $\mathbf{q}_{\text{pre}}$. For the inelastic event after elastic collision, they are, respectively, given by

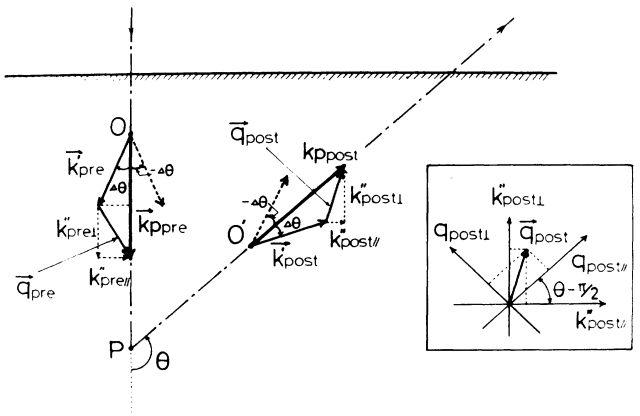

FIG. 11. Schematic diagram for a reflection electron energy-loss process. O and O' denote the inelastic events before and after elastic collision. P denotes the elastic collision. The suffixes, pre and post, are used to distinguish the events before and after elastic collision. $\mathbf{k}_p$ and $\mathbf{k}'_p$ are the wave vectors of the incident electron and the inelastic-scattered electron, respectively. $\mathbf{q}$ is the momentum transfer. θ and $\Delta\theta$ are the elastic and inelastic scattering angles, respectively. The total scattering angle is determined from the angular aperture of the CMA to be 137.7°. $k''_{\parallel}$ and $k''_{\perp}$ are the parallel and perpendicular components of the momentum transfer to the surface, respectively. $q_{\text{post}\parallel}$ and $q_{\text{post}\perp}$ in the inset are the parallel and perpendicular components of the momentum transfer with respect to the traveling direction. Among them the following relations hold. $k''_{\text{post}\parallel}=q_{\text{post}\parallel}\sin\theta+q_{\text{post}\perp}\cos\theta$ and $k''_{\text{post}\perp}=-q_{\text{post}\parallel}\cos\theta+q_{\text{post}\perp}\sin\theta$.

$$k''_{\text{post}\parallel} = k''_{\text{pre}\parallel}\cos\theta + k''_{\text{pre}\perp}\sin\theta \tag{6}$$

and

$$k''_{\text{post}\perp} = k''_{\text{pre}\parallel}\sin\theta - k''_{\text{pre}\perp}\cos\theta \ . \tag{7}$$

Equations (3)–(7) have been applied to the inelastic scattering processes involving excitation of inner-shell electrons of binding energies of 50, 150, and 450 eV as examples. The results are shown in Figs. 12–15, from which the following facts are found. (1) At small $\Delta\theta$ momentum transfer decreases monotonously with E_p, but at large $\Delta\theta$ it increases with E_p excluding the lower primary energy region. (2) The larger the energy loss, the larger is the momentum transfer. (3) When $\Delta\theta=0$, $k''_{\text{pre}\parallel}$ is identically zero because the momentum transfer vector turns to the direction of the wave vector of the normal incident electron. When $\Delta\theta\neq 0$, it increases monotonously with E_p from zero value at $E_p=\Delta E$ at the expense of $k''_{\text{pre}\perp}$. As a result the two curves intersect at certain primary energy. As ΔE decreases and/or $\Delta\theta$ increases, this intersection shifts to lower energy. (4) At small $\Delta\theta$, $k''_{\text{post}\parallel}$ ($k''_{\text{post}\perp}$) coincides approximately with $k''_{\text{post}\perp}$ ($k''_{\text{post}\parallel}$) at $-\Delta\theta$. Then if the inelastic events occur isotropically at small angles, they make a nearly equivalent contribution to the GOS.

In Sec. III we have pointed out that the ISEELS spectra measured at large E_p resemble the corresponding XAS and APS spectra. This fact may imply that dipole selection rules hold at large E_p. As can be seen from the fact (1) this condition is fulfilled only for inelastic scattering at small angle. Then the early assumption that the inelastic events occur in a forward direction and the energy losses observed during reflection from a surface are accompanied by large elastic collision seems reasonable.

The fact (3) may suggest that the ISEELS spectra measured at small E_p represent unoccupied energy states

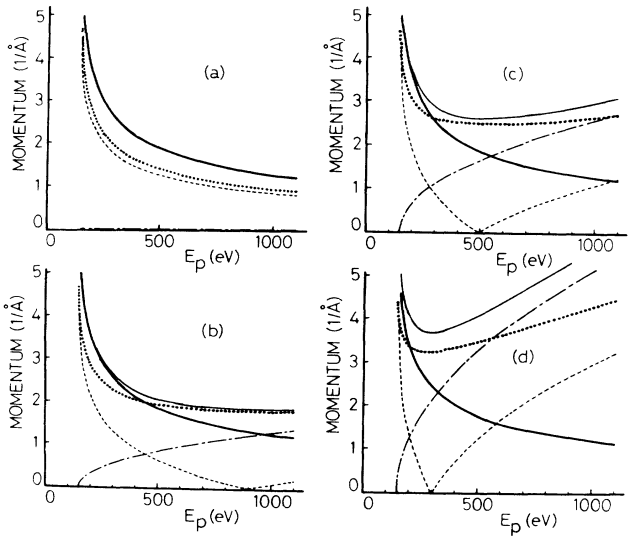

FIG. 13. Primary-energy dependence of the momentum transfer and its parallel and perpendicular components to the surface at $\Delta E=150$ eV; (a) $\Delta\theta=0°$, (b) $\Delta\theta=5°$, (c) $\Delta\theta=10°$, and (d) $\Delta\theta=20°$. A thin solid line represents the momentum transfer. A chain line and a thick solid line show the parallel and perpendicular components for the inelastic event before elastic collision, respectively, whereas a broken line and a dotted line show the parallel and perpendicular components after elastic collision, respectively.

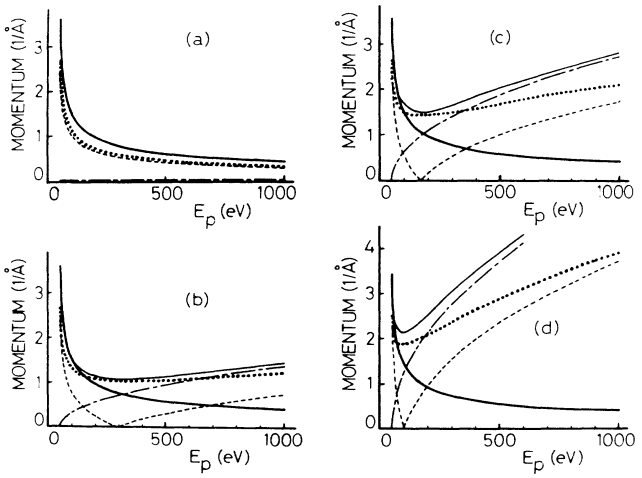

FIG. 12. Primary-energy dependence of the momentum transfer and its parallel and perpendicular components to the surface at $\Delta E=50$ eV; (a) $\Delta\theta=0°$, (b) $\Delta\theta=5°$, (c) $\Delta\theta=10°$, and (d) $\Delta\theta=20°$. A thin solid line represents the momentum transfer. A chain line and a thick solid line show the parallel and perpendicular components for the inelastic event before elastic collision, respectively, whereas a broken line and a dotted line show the parallel and perpendicular components after elastic collision, respectively.

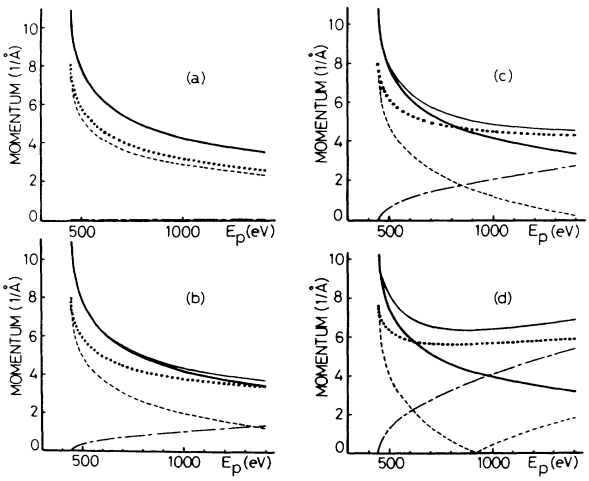

FIG. 14. Primary-energy dependence of the momentum transfer and its parallel and perpendicular components to the surface at $\Delta E=450$ eV; (a) $\Delta\theta=0°$, (b) $\Delta\theta=5°$, (c) $\Delta\theta=10°$, and (d) $\Delta\theta=20°$. A thin solid line represents the momentum transfer. A chain line and a thick solid line show the parallel and perpendicular components for the inelastic event before elastic collision, respectively, whereas a broken line and a dotted line show the parallel and perpendicular components after elastic collision, respectively.

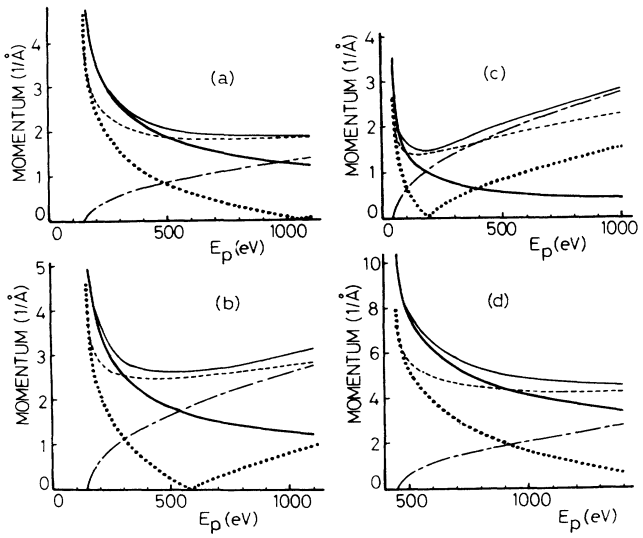

FIG. 15. Primary-energy dependence of the momentum transfer and its parallel and perpendicular components to the surface; (a) $\Delta E = 150$ eV and $\Delta\theta = -5°$, (b) $\Delta E = 150°$ eV and $\Delta\theta = -10°$, (c) $\Delta E = 50°$ eV and $\Delta\theta = -10°$, and (d) $\Delta E = 450$ eV and $\Delta\theta = -10°$. A thin solid line represents the momentum transfer. A chain line and a thick solid line show the parallel and perpendicular components for the inelastic event before elastic collision, respectively, whereas a broken line and a dotted line show the parallel and perpendicular components after elastic collision, respectively.

perpendicular to the surface dominantly, while the spectra at sufficiently large E_p represent unoccupied energy states parallel to the surface. This trend has been confirmed from the experimental results for graphite.[10] It is well known that the graphite σ^* antibonding band is derived from the orbitals parallel to the surface while the π^* antibonding band is derived from the orbitals perpendicular to the surface. Papagno and co-workers have found that at large E_p the σ^* antibonding peak is progressively enhanced relative to the π^* antibonding peak. The fact (3) also gives a reasonable explanation for the disappearance of the "d_{z^2}" peak observed in the S $L_{2,3}$ ISEELS spectrum in TaS_2 measured at large E_p as well. On the other hand, it does not seem that the variations of the ISEELS spectra for TiS_2 can be explained satisfactorily by only the consideration because the t_{2g} band contains not only the d_{z^2} orbitals perpendicular to the surface but also the $d_{x^2-y^2}$ and d_{xy} orbitals parallel to the surface. The calculations of the energy band structure and the density of states have been carried out for TiS_2 by many workers.[17,18,29–35] However, since the calculated densities of states are diverse and the ISEELS spectra may reveal the partial density of states, it is difficult to compare the peak intensities with the density of states obtained from the specific band calculation.

Here we may consider why the S $L_{2,3}$ and Ti $M_{2,3}$ spectra vary more rapidly with E_p, compared with the Ti $L_{2,3}$ spectrum. The momentum transfer multiplied by the radius of an inner-shell orbital are tabulated in Table I together with the parallel and perpendicular components. The radii of inner-shell orbitals were calculated with use of hydrogenlike wave functions. The value qr gives a criterion for the dipole approximation as seen from Eq. (2). A rough estimate shows that the quadrupole term contribution to the GOS is less than 10% of the dipole term contribution when qr is less than 0.3. As qr increases, quadrupole transitions are enhanced. From Table I we find that dipole selection rules approximately hold for the Ti $M_{2,3}$ spectrum at $E_p = 350$ eV and the S $L_{2,3}$ spectrum at $E_p = 500$ eV, but all the Ti $L_{2,3}$ spectra in Fig. 7 are out of the dipole approximation. Thus we may consider that the primary-energy dependence of the S $L_{2,3}$ and the Ti $M_{2,3}$ spectra arises from the transition from the dipole approximation to the multipole approximation including the quadrupole transitions. Taking the large variations of the parallel and perpendicular components of the momentum transfer into account, however, we cannot neglect the influence of the polarization effect. These affairs largely depend on the details of the angular distribution of inelastic events, the GOS, and the partial density of states, which have not yet been accurately determined. However, it is noted that in both cases the Ti $M_{2,3}$ and S $L_{2,3}$ spectra would vary more rapidly with E_p compared with the Ti $L_{2,3}$ spectrum.

V. CONCLUSIONS

The S $L_{2,3}$ and the Ti $M_{2,3}$ and $L_{2,3}$ ISEELS spectra in TiS_2 exhibited a doublet structure corresponding to the Ti $3d$ t_{2g} and e_g bands. The intensity ratio varied, depending on primary energy. At small E_p the t_{2g} peak

TABLE I. Momentum transfers and orbital radii of inner-shell electrons. q is the momentum transfer, r the orbital radius of an inner shell electron, $\Delta\theta$ the inelastic scattering angle, E_p the primary energy, and $k''_{\text{pre}\parallel}$ and $k''_{\text{pre}\perp}$ the parallel and perpendicular components of the momentum transfer, respectively.

Spectrum	Inner-shell electron	r (Å)	E_p (eV)	$\Delta\theta = 0°$ q (Å^{-1})	qr	$\Delta\theta = 10°$ q (Å^{-1})	qr	$k''_{\text{pre}\perp}r$	$k''_{\text{pre}\parallel}r$
Ti $M_{2,3}$	$3p$	0.37	80	1.78	0.67	1.89	0.70	0.65	0.18
			350	0.71	0.26	1.76	0.65	0.26	0.57
Ti $L_{2,3}$	$2p$	0.12	520	7.22	0.86	7.50	0.90	0.87	0.09
			940	4.37	0.53	4.95	0.59	0.51	0.24
S $L_{2,3}$	$2p$	0.17	220	3.31	0.56	3.46	0.59	0.56	0.13
			500	1.87	0.32	2.61	0.44	0.31	0.28

was predominated over the e_g peak. The similar variation was found for the S $L_{2,3}$ ISEELS spectrum in TaS_2. In this case the first peak which corresponds to the "d_{z^2}" band disappears at large E_p. These variations were discussed primarily in terms of the momentum transfer involved in the excitation process of an inner-shell electron to unoccupied energy states, its parallel and perpendicular components to the surface, and anisotropy in electronic structures. The main results obtained are summarized as follows.

(1) Inelastic events in the reflection inner-shell-electron energy-loss process are accompanied by large elastic collision so that electrons are inelastically-scattered dominantly in a forward direction.

(2) Dipole selection rules approximately hold for the reflection ISEELS spectra at sufficiently large E_p, while at small E_p they are relaxed due to increased momentum transfer.

(3) In the system used here electronic states parallel and perpendicular to the surface may be distinguished from the primary-energy dependence. The perpendicular component of the momentum transfer is predominant over the parallel component at small E_p, but decreases with E_p. On the contrary, the parallel component increases with E_p.

(4) The primary energy dependence of the ISEELS spectra for layered transition-metal dichalcogenides may result from the breakdown of dipole selection rules and/or anisotropy in electronic band structures.

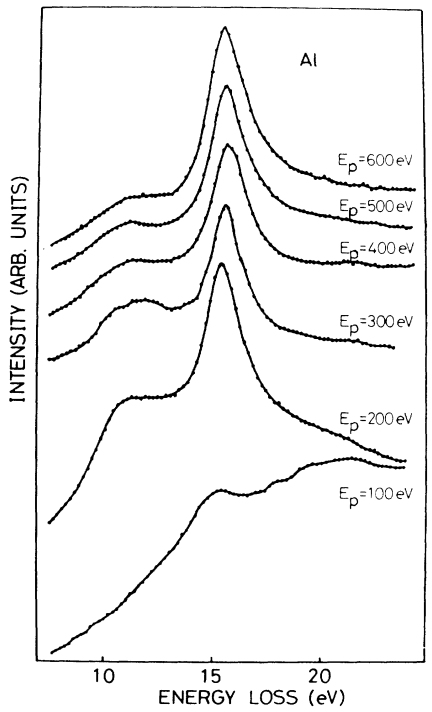

FIG. 16. Plasmon-excitation energy-loss spectra for aluminum at various incident energies. They were measured in the pulse-counting mode in reflection geometry at normal incidence.

ACKNOWLEDGMENTS

This work is partially supported by a Grant-in-Aid for Scientific Research from the Ministry of Education, Science and Culture of Japan.

APPENDIX

Here we give the evidence that forward inelastic scattering makes a dominant contribution to reflection energy-loss spectra. Figure 16 shows the plasmon excitation energy-loss spectra for aluminum. These spectra have been measured in the pulse-counting mode as a function of primary energy. It is known that plasma frequency or plasmon excitation energy changes with momentum transfer. Its relation is given in the free-electron approximation by[36]

$$\hbar\omega_p(q)=\hbar\omega_p(0)+Aq^2 \tag{A1}$$

and

$$A=\frac{3\hbar E_f}{5m\omega_p(0)} . \tag{A2}$$

Here $\omega_p(0)$ are the plasma frequency at $q=0$ and E_f is the Fermi energy. In practice Gibbons *et al.*[37] confirmed that the plasmon excitation energy increases linearly with q^2 until momentum transfer reaches the cutoff wave vector $q_c=1.3$ Å^{-1}, the proportional constant A being about 3.2, in agreement with the theoretical value (3.4). The application of the relation to our cases gives the momentum transfer less than 0.12 Å^{-1}. Gibbons *et al.* have also indicated that the peak width increases linearly with q^2. The application of this result to our cases gives the momentum transfer less than 0.6 Å^{-1}. The difference of the values may arise from the fact that the peak energy reflects the energy at a dominant momentum transfer while the width is the integrated width over various momentum transfers. For the primary energies of 100–600 eV and the energy loss of 15 eV, Eq. (3) gives the momentum transfers of 0.4–0.16 Å^{-1} at $\Delta\theta=0°$ and 1.73–2.17 Å^{-1} at $\Delta\theta=10°$, respectively. Hence we may conclude that the inelastic events occur dominantly at small scattering angle.

[1]*Electron Energy-Loss Spectroscopy in the Electron Microscopy*, edited by R. F. Egerton (Plenum, New York, 1986).

[2]C. J. Powell and N. E. Erickson, Phys. Rev. Lett. **51**, 61 (1983).

[3]Y. Sakisaka, T. Miyano, and M. Onchi, Phys. Rev. Lett. **54**, 714 (1985).

[4]J. Kanski and P. O. Nilsson, Phys. Rev. Lett. **43**, 1185 (1979); J. Kanski and G. Wendin, Phys. Rev. B **24**, 4977 (1981).

[5]J. A. Matthew, G. Strasser, and F. P. Netzer, Phys. Rev. B **27**, 5839 (1983); G. Strasser, F. P. Netzer, and J. A. D. Matthew,

Solid State Commun. **49**, 817 (1984).
[6]J. M. Esteva and R. C. Karnatak, Phys. Rev. Lett. **50**, 910 (1983).
[7]F. P. Netzer, G. Strasser, and J. A. D. Matthew, Phys. Rev. Lett. **51**, 211 (1983).
[8]R. D. Leapman and J. Silcox, Phys. Rev. Lett. **42**, 1361 (1979); R. D. Leapman, R. L. Fejes, and J. Silcox, Phys. Rev. B **28**, 2361 (1983).
[9]S. Saito, K. Higeta, and T. Ichinokawa, J. Microscopy **142**, 141 (1986).
[10]L. Papagno and L. S. Caputi, Surf. Sci. **125**, 530 (1983); L. Papagno, L. S. Caputi, M. De Crescenzi, and R. Rosei, Phys. Rev. B **26**, 2320 (1982).
[11]*Physics and Chemistry of Materials with Layered Structures,* (Reidel, Dordrecht, Holland, 1977–1979), Vols. 1–6.
[12]Y. Ohno, Bull. Fac. Gen. Educ. Utsunomiya Univ. Sec. 2 **19**, 5 (1986).
[13]J. A. Bearden and A. F. Burr, Rev. Mod. Phys. **39**, 125 (1967).
[14]M. Cardona and L. Ley, *Photoemission in Solid I* (Springer, New York, 1978).
[15]R. D. Leapman, L. A. Grunes, and P. L. Fejes, Phys. Rev. B **26**, 614 (1982).
[16]Y. Ohno, K. Hirama, S. Nakai, C. Sugiura, and S. Okada, Phys. Rev. B **27**, 3811 (1983).
[17]A. Zunger and A. J. Freeman, Phys. Rev. B **16**, 906 (1977).
[18]G. A. Benesh, A. M. Woolley, and C. Umrigar, J. Phys. C **18**, 1595 (1985).
[19]D. W. Fischer, Phys. Rev. B **8**, 3576 (1973).
[20]C. Webb, Vacuum **27**, 537 (1977).
[21]L. F. Mattheiss, Phys. Rev. B **8**, 3719 (1973).
[22]B. Sonntag and F. C. Brown, Phys. Rev. B **10**, 2300 (1974).
[23]D. Straub, M. Skibowski, F. J. Himpsel, and W. Drube, Phys. Rev. B **31**, 8254 (1985).
[24]S. Nakai, K. Ogata, C. Sugiura, T. Mitsuishi, and H. Maezawa, J. Phys. Soc. Jpn. **54**, 4034 (1985).
[25]M. Campagna, G. K. Wertheim, and Y. Baer, in *Topics in Applied Physics,* edited by L. Ley and M. Cardona (Springer-Verlag, Berlin, 1979), Vol. 27, p. 217.
[26]L. Vriens, J. A. Simpson, and S. R. Mielczarek, Phys. Rev. **165**, 7 (1968).
[27]R. D. Leapman, P. Rez, and D. F. Mayers, J. Chem. Phys. **72**, 1232 (1980).
[28]A. G. Nassiopolous and J. Cazaux, Surf. Sci. **165**, 203 (1986).
[29]R. B. Murray and A. D. Yoffe, J. Phys. C **5**, 3038 (1972).
[30]H. W. Myron and A. J. Freeman, Phys. Rev. B **9**, 481 (1974).
[31]P. Krusius, J. von Boehm, and H. Isomaki, J. Phys. C **8**, 3788 (1975).
[32]D. W. Bullet, J. Phys. C **11**, 4501 (1978).
[33]H. Isomaki, J. von Boehm, and P. Krusius, J. Phys. C **12**, 3239 (1979); H. Isomaki and J. von Boehm, *ibid.* **14**, L75 (1981).
[34]F. Antonageli, M. Piacentini, R. Girlanda, G. Martino, and E. S. Giuliano, Phys. Rev. B **32**, 6644 (1985).
[35]T. Yamazaki, N. Suzuki, and K. Motizuki (private communication).
[36]H. Raether, in *Springer Tracts in Modern Physics,* edited by G. Hohler (Springer-Verlag, Berlin, 1980), Vol. 88, p. 74.
[37]P. C. Gibbons, S. E. Schnatterly, J. J. Ritsko, and J. R. Fields, Phys. Rev. B **13**, 2451 (1976).